AEROELASTIC INVESTIGATION OF HINGELESS HELICOPTER BLADES WITH INTEGRATED SMART MORPHING ACTUATOR

C. Testa[1], S. Leone[1], J. Serafini[2], and M. Gennaretti[2]

[1]CIRA - Italian Aerospace Research Center
Via Maiorise snc, 80143 Capua (CE), Italy
e-mail: c.testa@cira.it

[2]Mechanical & Industrial Eng. Dept., University Roma Tre
Via della Vasca Navale 79, 00146 Rome, Italy
e-mail: m.gennaretti@uniroma3.it

Key words: Blade morphing, Smart structures, Aeroelastic stability.

Abstract. This paper deals with the aeroelastic analysis of a hingeless helicopter blade smarted with a morphing system aimed to the reduction of BVI noise through transformation of the blade tip shape into an anhedral tip type. The proposed actuation system is based on a variable-stiffness device coupled with the actions provided by inertial moments and shape memory alloys (SMA) tie-rods. Since the inertial moments are provided by a suitable mass distribution and the smart system effectiveness is strongly dependent on the amount of it, this work focuses the attention on the resulting modified dynamic and aeroelastic blade responses. In particular, the numerical investigation examines the aeroelastic stability and the rotating frequencies of vibration of the smarted blade, comparing them with those of the baseline configuration. Potentiality and shortcomings of the smarted blade are analysed and possible alternative solutions, as well as, envisaged further improvements are discussed.

1 INTRODUCTION

In the last years, the rotorcraft community has devoted considerable efforts toward the enhancement of helicopter performances by integrating smart systems into the main rotor blades. Blade morphing is one of the techniques that may be applied to this aim. However, the extremely complex environment related to rotating blades affects the capability of it. The high energy required and the significant displacements and forces involved, make some engineering solutions aimed to guarantee light-weight and adaptivity unpractical. Thus, their practical application is currently limited to few approaches.

The smart system based on blade morphing examined here is devoted to the reduction of the noise generated, which is one of the critical issues related to helicopter (main rotor) performance and certification, because of the extremely annoying effects that deeply limit the widespread operation of helicopters in populated areas. In particular, in low-speed descent flight (and sometimes in hovering or fly-over conditions), the acoustic annoyance produced by aerodynamically generated noise is mainly due to the blade-vortex interaction phenomenon (BVI). It occurs when strong blade tip vortices impinge or pass closely to the following rotor blades, resulting in impulsive changes of the blade loads that, in turn, produce high noise and vibration levels. A possible strategy to alleviate the BVI noise is to diffuse the blade tip vortex, or displace it far away from the following

blades by increasing the blade vortex miss-distance. Such a solution may be achieved through an anhedral tip shape; previous research[1,2] has shown that typically, the tip vortex involved in the blade-vortex impinging is related to a spanwise lenght of about $10-15\%$ of the span and noise is attained if a mean slope variation of $5°$, at least, is achieved. Some of the authors have faced the problem of transforming the blade tip region into an anhedral shape in the past[3,4] showing that blade morphing may be achieved by exploiting the energy of the centrifugal field and not only through the actions provided by the actuators based on piezoelectric materials (PZT), shape memory alloys (SMA), ect. In that activity, an innovative integrated smart stiffness-variable system is examined and a feasibility study is addressed to investigate its potentiality. As it is shown in Refs. 3 and 4, the stiffness variation is allowed by a magneto-rheological device (MRF) located just behind the controlled zone, estimated in $10-15\%$ of span. Once the MRF is switched-on, the bending moments provided by eccentric masses, properly distributed inside the blade-box, and the action of a SMA-based actuator, allow to morph the blade tip. By increasing the amount of concentrated masses, a higher morphing action is expected. Anyway, as discussed in Ref. 3, this is not a reasonable way for improving the performances of the proposed smart-architecture since the limitation of fuselage vibration loads as well as the aeroelastic stability of the rotor blades have to be assured for any flight condition.

For these reasons, this paper is devoted to a numerical investigation on the aeroelastic behavior of the proposed smarted main-rotor. Although also descent flight and fly-over conditions should be studied, in this work only the attention is focused on the hover condition in order to derive some guidelines on effects of the smart system proposed on the aeroelastic stability of the blades. To perform the aeroelastic analysis, the linearized equations for small perturbation motions about the equilibrium operating condition are derived and the eigenanalysis is accomplished. To this aim, the blade is modelled as an isotropic, elastic, non-uniform rotating beam undergoing lead-lag, flap and torsion displacements, whereas the aerodynamic loads are given by a strip-theory approach based on a quasi-steady approximation of the Greenberg theory. Spanwise actions induced by the integrated smart system are modelled as concentrated moments. The Finite Element Method (FEM) is used to determine the equilibrium blade deflections, while the perturbation equations are obtained through application of the Galerkin approach.

2 ACTUATION SYSTEM AND FORCES

The actuation system under consideration, aimed to achieve an anhedral blade tip shape, is fully described in Refs. 3 and 4; anyway, for the sake of clarity, some important features and the selection of configuration parameters are here outlined.

The typical problem of any smart structure consists of preserving the necessary robustness with the addition of some labilities to get the required shape. The innovative smart architecture proposed in Refs. 3 and 4 is based on a quite new way of thinking in the framework of the actuation systems for rotating blades. Indeed, it combines the advantages of an adaptive stiffness beam with the energy developed by the rotating enviromnent when eccentric masses are properly located into the blade box. In details, the capability to morph the blade tip is based on an on-off system composed of a magneto-rheological fluid-based device (MRF), a shape memory alloy ribbon-based device (SMA) and a set of concentrated masses properly distributed inside the blade box (see figure 1). The MRF system provides a spanwise local control of the bending stiffness, whereas the SMA ele-

ments, combined with the forces induced by the concentrated masses, bend the structure. When the anhedral shape is needed the intensity of the magnetic field is decreased thus reducing the bending stiffness, concentrated masses are suitably displaced and the SMA elements are switched on. In such a way, the joint bending actions of concentrated masses and SMA actuator deflects the blade tip region. Once the required anhedral shape is achieved, the SMA device is switched off and the magnetic field is incresed until the equilibrium configuration is frozen. When no anhedral configuration is needed a magnetic field is applied to the MRF device so that the fluid viscosity increases and the blade controlled zone is completely locked. In this case, the SMA tie-rod is switched off and the masses are still located in their rest positions.

In the following, the above actuation strategy is discussed. Apparently, there is no reason why it is required the coupled action of three different devices to achieve the blade morphing. As it is shown in Ref. 3, if the only MRF device is applied, the geometrical blade configuration remains very close to the non-actuated one even for a stiffness variation, K_{MRF}, equal the 65% of the initial stiffness. However, for K_{MRF} equal to the 75% of the initial stiffness a slope variation, $\Delta\theta = -0.11°$ is achieved between $x = 0.9R$ and the blade tip. On the other hand, the investigation on the effects due only to the SMA actuator reveals that the corresponding flap bending moments have the capability to modify the structure. The best configuration is achieved when the maximum allowable number of ribbons, computed with reference to the internal space, is used. For the blade considered in Refs. 3 and 4 having a NACA 0015 airfoil, 30 ribbons providing a $15KN$ force, produce a slope variation $\Delta\theta = -0.24°$. Coupling the MRF device with the SMA actuator, the advantages of local stiffness reduction are exploited. However, in this case, the weakening provided by the MRF cannot be too large, and the numerical investigations[3] show that for a realistic four-bladed rotor, K_{MRF} has to be not greater than the 50% of the initial stiffness in order to avoid transforming the blade tip into a real hinged-beam and experiencing too large blade tip displacements. Limiting K_{MRF} to the 50% of the initial stiffness, the combined action of MRF and SMA yields $\Delta\theta = -0.26°$. Anyway, the resulting blade tip shape does not match the required one even if SMA device is applicated at the maximum of its capability.[3] This problem may be overcome by exploiting the actions induced by the centrifugal field. As a matter of fact, by using a set of concentrated masses properly located inside the blade box above the elastic axis, the resulting bending moments induced by the centrifugal forces are able to modify the blade shape. As it is shown in Ref. 3, to this purpose at least three masses are required; m_1 aimed to improving the effect of the MRF-SMA device, m_2 to allow moulding the blade shape whereas M, located at the blade tip, to modify the blade shape for achieving the targeted anhedral configuration. It is worth noting that in the MRF-SMA-based actuation system, shape memory alloys are called to bend the outer portion of the blade while through the use of concentrated masses, the centrifugal field is devoted to yield the major bending effect being the SMA actuator used to provide a local bending

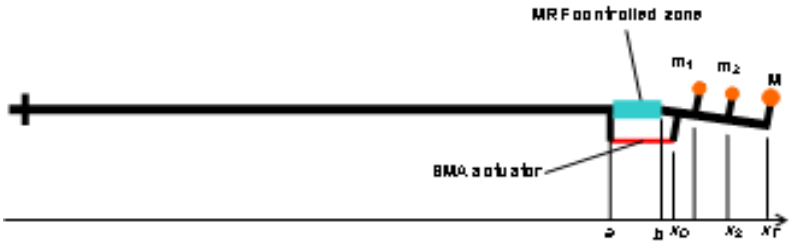

Figure 1: sketch of the smart system.

slope change in the area where the MRF device acts (so that the characteristc beak profile is obtained). In details, by using $m_1 = m_2 = 0.25Kg$ and $M = 1.5Kg$ (corresponding to a mass increase that is equal to the 8% of the blade mass), for K_{MRF} equal to the 50% of the initial stiffness and using 15 SMA ribbons, the bending slope variation obtained in Ref. 3 is $\Delta\theta = -2.2°$, which corresponds to the 44% of the requirement ($\Delta\theta = -5°$, see Refs. 1 and 2). This result should be improved by increasing the amount of concentrated masses or the SMA ribbons or decreasing the stiffness in the controlled zone. Anyway, the satisfaction of the requirement is well beyond the scope of that investigation because the purpose of that work was to address a feasibility study on a realistic helicopter rotor, in order to study the capabilities of the proposed integrated system and derive some useful and preliminary guidelines on the rotorcraft blade morphing.

3 AEROELASTIC MODEL OF THE ACTUATED HINGELESS BLADE

The capability of an integrated smart system to change the blade shape in hovering depends on the coupling beewten aeroelastic loads and actuation forces. Thus, a phisically-consistent aeroelastic model has to include all the actions induced by the actuators embedded into the elastic structure. The aeroelastic formulation used in this work is briefly outlined here. More details can be found in Refs. 5 and 6. The equations governing blade aeroelasticity are obtained by coupling the equations of the blade dynamics introduced in Ref. 6 with the aerodynamic loads given by a quasi-steady 2D theory. Although the aerodynamic model used in this investigation is quite simple, it is commonly used by helicopter industries for evaluating the blade response at very low frequency analysis. To take into account the 3D trailing vortices effect, wake-inflow correction is included.[7] The rotor blade is modelled as a long, straight, slender, homogeneous isotropic beam; the theory is intended for moderate displacements, accurate to second order, and based on the hypothesis that squares of bending slopes, twist, thickness-radius and chord-radius ratios are small with respect to unity. Radial non-uniformities (mass, stiffness, etc.), chordwise offsets of the mass centroid and tension axes from the elastic axis, pre-cone and warping are included; other details, such as blade root feathering flexibility, torque offset, blade sweep and droop are not herein considered. Eliminating the radial displacement from the set of equations by solving it in terms of local tension, the equations governing the steady aeroelasticity of an actuated hovering blade may be written as

$$
\begin{aligned}
&-[v'\Omega^2 \int_x^R \mu\, x\, \mathrm{d}x]' + \left\{ \left[EI_z - \Delta K\, \sin^2(\theta+\phi) \right] v'' + \frac{1}{2}\Delta K \sin 2(\theta+\phi) w'' \right\}'' + \\
&-\mu\Omega^2[v + e\cos(\theta+\phi)] - [\mu\,(e-e_A)\,\Omega^2\, x\, \cos(\theta+\phi)]' = L_v \\
&\\
&-[w'\Omega^2 \int_x^R \mu\, x\, \mathrm{d}x]' + \left\{ \left[EI_y - \Delta K\, \sin^2(\theta+\phi) \right] w'' + \frac{1}{2}\Delta K\, \sin 2(\theta+\phi) v'' \right\}'' + \\
&-[\mu\,(e-e_A)\,\Omega^2\, x\, \sin(\theta+\phi)]' + \mu\,\Omega^2\,\beta_{pc}\, x = L_w + F_w^{act} \qquad (1) \\
&\\
&-k_A^2\Omega^2[(\theta+\phi)' \int_x^R \mu\, x \mathrm{d}x]' + \Delta K\,[v''w''\cos 2\theta + (w''^2 - v''^2)\frac{\sin 2\theta}{2}] \\
&+\mu\, e\,\Omega^2 x(w'\cos\theta - v'\sin\theta) - (GJ\phi')' + \mu\,\Omega^2\,\phi\,(k_{m_2}^2 - k_{m_1}^2)\cos 2\theta + \mu\, e\,\Omega^2\beta_{pc}\, x\, \cos\theta \\
&-e_A\Omega^2(w''\cos\theta - v''\sin\theta)\int_x^R \mu\, x\, \mathrm{d}x + \mu\,\Omega^2(k_{m_2}^2 - k_{m_1}^2)\cos\theta\sin\theta = M_\phi + M_\phi^{act}
\end{aligned}
$$

where the unknowns are the in-plane (lead-lag, v) and the out-of-plane (flap, w) displacements of the elastic axis, as well as the cross-section torsion, ϕ, around it. Bending and

torsional stiffness are represented by EI_z, EI_y and GJ respectively ($\Delta K = EI_z - EI_y$), μ is the blade mass for unit length and x the spanwise position. In addition, k_{m_1} and k_{m_2} are the principal mass radii of gyration, k_A the blade cross-section polar radius of gyration, β_{pc} the pre-cone angle, e the offset of the center of mass from the elastic axis and e_A the tension axis offset from the elastic axis.

The forcing terms at the right-hand side of equation (1) are the sum of the loads given by the actuation device (F_w^{act} and M_ϕ^{act}) with the sectional aerodynamic loads (L_v, L_w and M_ϕ). From the description of the smart system given in Section 2, the actuation loads come from the localized bending moments exerted by the action of eccentric masses and SMA tie rods and reads (no lagwise actuation load arises)

$$\begin{aligned} F_w^{act} &= \Omega^2 \frac{\hat{t}}{2} \left[m_1 \delta'(x - x_1) x_1 + m_2 \, \delta'(x - x_2) x_2 + M \delta'(x - x_T) \, x_T \right] \\ &- F_{sma} \, b \left[\delta'(x - x_c) - \delta'(x - x_d) \right] \\ M_\phi^{act} &= \Omega^2 \frac{\hat{t}}{2} \left[m_1 \delta'(x - x_1) x_1 \, v_1' + m_2 \delta'(x - x_2) x_2 \, v_2' + M \delta'(x - x_T) x_T \, v_T' \right] \\ &- F_{sma} \, b \, \delta' \left[(x - x_c) v_c' - (x - x_d) v_d' \right] \end{aligned}$$

In the equations above m_k is the k-th concentrated mass located at the abscissa x_k on the elastic axis, M is the tip mass, $\hat{t}$ denotes a portion of the cross-section thickness, v_k' is the lag-bending slope at x_k, F_{sma} is the axial force provided by the SMA actuator, b is the arm with respect to the beam axis and Ω is the rotor angular velocity.

Concerning the aerodynamic loads, the lagwise section load, L_v, the flapwise section load, L_w, and the sectional pitching moment about the elastic center, M_ϕ, for a steady-state hovering configuration are given by

$$\begin{aligned} L_v &= \frac{\rho \, a \, c}{2} [v_i^2 - \Omega^2 \, x^2 \, \frac{c d_0}{a} - \Omega \, x \, v_i \, (\theta + \phi)] \\ L_w &= \frac{\rho \, a \, c}{2} [-\Omega \, x \, v_i + \Omega^2 \, x^2 \, (\theta + \phi + \int_0^x v' \, w'' \mathrm{d}x) + \Omega^2 \, \frac{x \, c}{2} (\beta_{pc} + w') - \Omega^2 \, x \, v (\beta_{pc} + w')] \\ M_\phi &= e_d \, L_w \end{aligned}$$

where ρ denotes air density, c is the local chord, a is the airfoil lift curve slope, v_i the local induced velocity and e_d the chordwise offset of the aerodynamic center behind the elastic axis. Wake effects are taken into account through the following model for the induced velocity, v_i,[7]

$$v_i = sgn[\theta + \phi_{75}] \Omega R \frac{\sigma \pi}{8} \left[\sqrt{1 + \frac{12}{\sigma \pi} |\theta + \phi_{75}|} - 1 \right]$$

where $\sigma = N_b \, c / \pi R$ is the blade solidity.

3.1 Steady equilibrium configuration

The finite element method (FEM) is used for the integration of equations (1) that yields the equilibrium blade configuration around which the aeroelastic stability may be investigated. To this aim, the blade is divided into N beam-elements, each having three nodes (two boundary and an interior one) and 11 degree of freedoms (dof's). Each boundary node (of any element) is characterized by 5 dof's (v, v', w, w', ϕ) while the internal one

is used for taking into account the elastic twist, only. Thus, for lag and flap bending deflections the interpolating polynomial is chosen from the family of Hermite's polynomials whereas lagrangian polynomials are used for the elastic twist. For the i-th beam-element, the introduction of the matrix shape functions $\mathbf{H}(x)$, yields the local field displacement as $\mathbf{u}_e(x) = \mathbf{H}(x)\,\mathbf{q}_e$, where $\mathbf{q}_e$ represents the elemental nodal displacement vector defined as $\mathbf{q}_e^T = [v_i, v_i', v_j, v_j', w_i, w_i', w_j, w_j', \phi_i, \phi_k, \phi_j]$. Finally, the application of the FEM method transforms equations (1) into the following discretised form

$$\mathbf{K}\mathbf{q} = \mathbf{F}_0 + \mathbf{F}_{NL}(\mathbf{q}) \tag{2}$$

where $\mathbf{q}$ denotes the vector collecting the degrees of freedom of all elements. At the left-hand side, $\mathbf{K}$ is the aeroelastic stiffness-matrix deriving from the linear contribution of aerodynamics and structural loads, including the centrifugal stiffening, whereas the global nodal loads $\mathbf{F}_0$ and $\mathbf{F}_{NL}$, at the right-hand side, account for constant and nonlinear terms from aerodynamics, structure and actuation. The solution of equation (2) is obtained iteratively through the application of the Newton-Raphson method that, at the k-th iteration, yields

$$(\mathbf{K} - \left.\frac{\partial \mathbf{F}_{NL}}{\partial \mathbf{q}}\right|_k)\mathbf{q}^{k+1} = \mathbf{Q}_0 - \left.\frac{\partial \mathbf{F}_{NL}}{\partial \mathbf{q}}\right|_k \mathbf{q}^k \tag{3}$$

Finally, note that the vehicle weight W must be balanced by the rotor thrust T: the elastic displacements and the collective angle corresponding to the equilibrium conditions are determined jointly by solving equation (3) coupled with the trim equation $T - W = 0$.

3.2 Stability Analysis

In order to investigate the blade aeroelastic stability, the equations of the blade dynamics (1) with the inertial terms included are integrated by application of the Galerkin method. To this aim, the blade elastic displacements are expressed in terms of the following series of generalized coordinates and mode shape functions

$$\begin{aligned} v(x,t) &= \sum_{j=1}^{N} V_j(t)\,\Psi_j(x) \\ w(x,t) &= \sum_{j=1}^{N} W_j(t)\,\Psi_j(x) \\ \phi(x,t) &= \sum_{j=1}^{N} \phi_j(t)\,\Theta_j(x) \end{aligned}$$

where Ψ_j and Θ_j are, respectively, bending and torsion non-rotating, uncoupled mode shapes of a uniform cantilever beam. This operation yields $3N$ nonlinear, nonhomogeneous, constant-coefficient ordinary differential equations in terms of modal generalized coordinates V_j, W_j and ϕ_j. Then, these are linearized for small perturbation motion about the equilibrium operating condition by expressing the lagrangean coordinates in terms of the superposition of steady equilibrium quantities and small unsteady perturbations quantities

$$\begin{aligned} V_j(t) &= V_{0_j} + \Delta V_j(t) \\ W_j(t) &= W_{0_j} + \Delta W_j(t) \\ \phi_j(t) &= \phi_{0_j} + \Delta \phi_j(t) \end{aligned}$$

with V_{0_j}, W_{0_j} and ϕ_{0_j} determined from the steady-state FEM solution outlined above (a least-square procedure is applied to this aim). The $3N$ resulting constant-coefficient equations that define the unsteady blade motion near the equilibrium configuration may be recast in the usual matrix form

$$\mathbf{M}\ddot{\mathbf{x}} + \mathbf{C}\dot{\mathbf{x}} + \mathbf{K}\mathbf{x} = \mathbf{0}$$

where the $3N \times 3N$ matrices depend on V_{0_j}, W_{0_j} and ϕ_{0_j} and $\mathbf{x}^T = [\Delta V_j, \Delta W_j, \Delta\phi_j]$, and the stability is investigated through the standard eigenvalue technique. Note that the smart system applied affects the perturbation equation both through the influence on the steady equilibrium condition and explicitly through terms of the torsion equation appearing in the stiffness matrix.

4 NUMERICAL RESULTS

Before showing the aeroelastic stability analysis for a hingeless blade controlled by the variable-stiffness device described above, some numerical results are shown to validate the methodology of Section 3.1 through which steady responses are obtained. To this aim, the untwisted cantilever blade considered in Ref. 8 has been examined. It has uniform mass and stiffness distribution, and no offsets between elastic, mass, tension and aerodynamic axes. Figure 2 shows the steady-state tip deflections computed for $\beta_{pc} = -5°$ for different collective angles and demonstrates that the agreement with the solution given in Ref. 8 (circles) is excellent.

Next we discuss the application of the smart morphing device. First, we present its capability to change the shape of the blade tip, considering a Bo105-type four-bladed rotor having a NACA 0015 cross-section and rotational speed $\Omega = 44 rad/sec$, that has been derived from Ref. 9. The smart system configuration applied has been obtained by a preliminary study. The outcome of it was that for an efficient use of the system the SMA actuator has to be positioned between $0.87R$ and $0.92R$ while the MRF device between $0.87R$ and $0.9R$. Indeed, by using 13 ribbons providing a $6500N$ force, imposing a bending stiffness reduction K_{MRF} equal to 50% of the initial stiffness and applying a concentrated masses configuration with $M = 1.5Kg$ and $m_1 = m_2 = 0.5Kg$ added to a uniformly distributed mass equal to $0.5Kg$ between $x_1 = 0.92R$ and $x_2 = 0.97R$ (see figure 1), a beak profile is obtained for the fully-actuated blade. This is shown in figure 3, where the trim flap displacement is depicted for the basic blade, the non-actuated (SMA and MRF switched-off) blade with two tip mass locations, and the fully-actuated blade. These results suggests two observa-

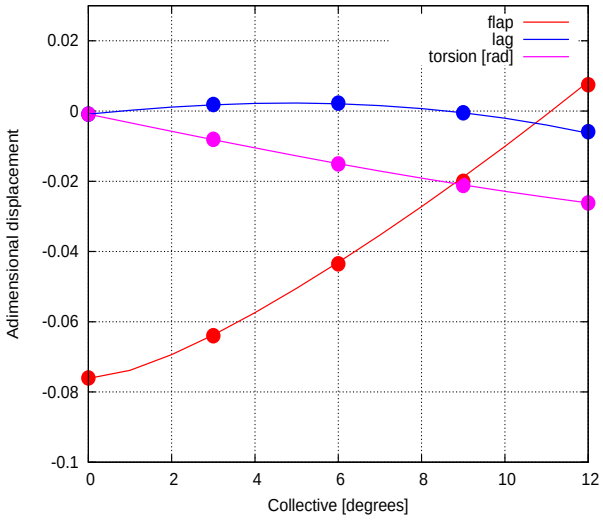

Figure 2: equilibrium blade tip deformation.

tions: (i) locating the masses distribution on the elastic axis make the blade tip region bend because of the centrifugal effects and thus, when the tip morphing is not required the masses has to be located at the lower side of the blade box (see blue line in figure 3); (ii) only the combined action of tip masses, SMA and MRF yields the tip beak profile (fully-actuated system). This latter issue is particularly examined in figure 4 where the effectiveness of the integrated variable stiffness device is shown. A significant tip blade deformation is obtained by the combined action of masses (moved upwards) and MRF, but the best blade morphing of the outer $10 - 15\%$ portion of the span is achieved by using the joint action of SMA, MRF and masses. The amount of additional mass included

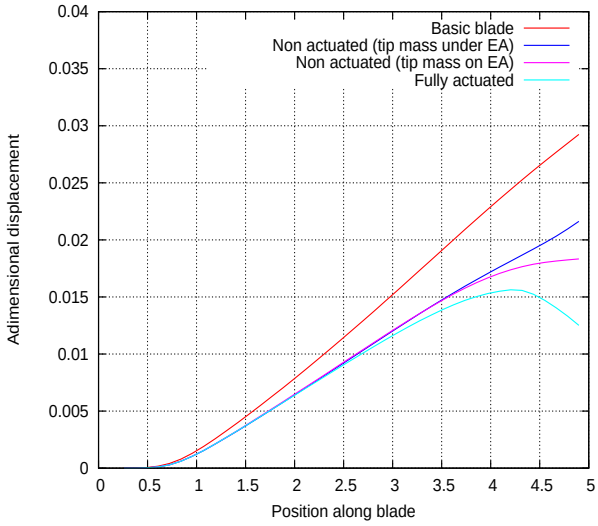

Figure 3: mass effect on blade flap deformation.

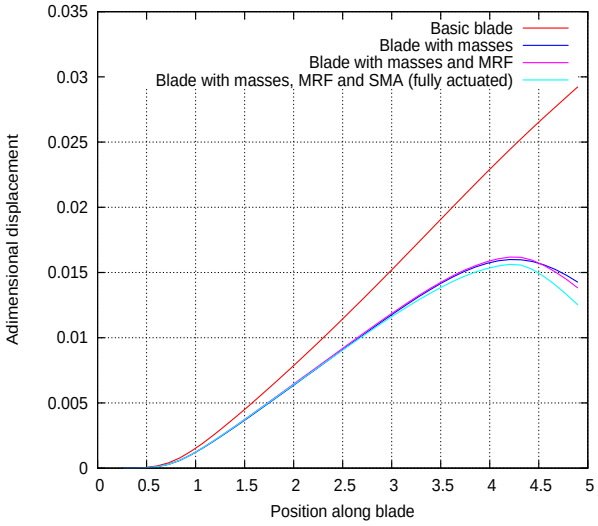

Figure 4: smart device effect on blade flap deformation.

in the configuration examined does not overcome the 11% of the basic blade mass and is the result of an optimization study aimed to amplify the bending effect of the centrifugal field.

However, the goal of tip blade morphing has to be matched both with the aimed BVI noise abatement and with the requirements concerning the rotor dynamic response. In particular, the modified dynamic response has to be such that blade resonances and aeroelastic instabilities are avoided within the field of operative conditions. Here, being the study of the noise abatement due to blade morphing beyond the scope of the present paper, the emphasis is on the analysis of the effects of the integrated smart system on the aeroelastic behavior of the blade. The stability analysis concerning the smarted blade yielding the results in figures 3 and 4 shows that it is unstable and that the aeroelastic behavior strongly depends on the value of the tip mass M, while the effect of m_1 and m_2 is almost negligible. Thus, the smarted blade has been re-designed in order to avoid aeroelastic instabilities. The numerical investigation has demonstrated that the stability is assured if the tip mass do not exceed the value of $M = 0.4Kg$ (about the 70% reduction), for $m_1 = m_2 = 0.2Kg$ in addition to a uniformly distributed mass equal to $0.78Kg$ located between x_1 and x_2. Unfortunately, the blade morphing effect produced by such configuration of the smart system is reduced and, in order to get a tip shape similar to that given by the higher-mass configuration, a second SMA actuator has been located close to the blade tip (see figure 5). Through this actuation strategy it has been proven that,

keeping m_1, m_2 and the mass between them constant, the blade equilibrium configuration does not change for tip mass values between $0.25Kg$ and $0.4Kg$ (see figure 6). The SMA-based actuation device has to produce a $12500N$ force (25 ribbons) when $M = 0.4Kg$, while a $14000N$ force (28 ribbons) is needed when $M = 0.25Kg$. Higher mass reduction is not allowed since 30 ribbons is approximately the maximum value for cross-sections typically used in conventional helicopter blades.

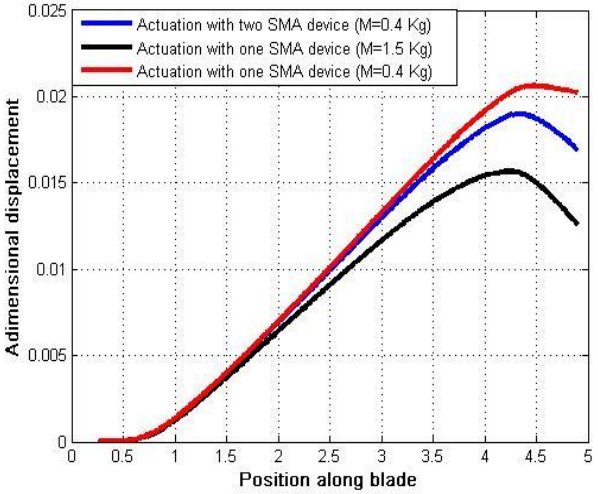

Figure 5: blade flap deformation using one and two SMA actuators. $M = 0.4Kg$.

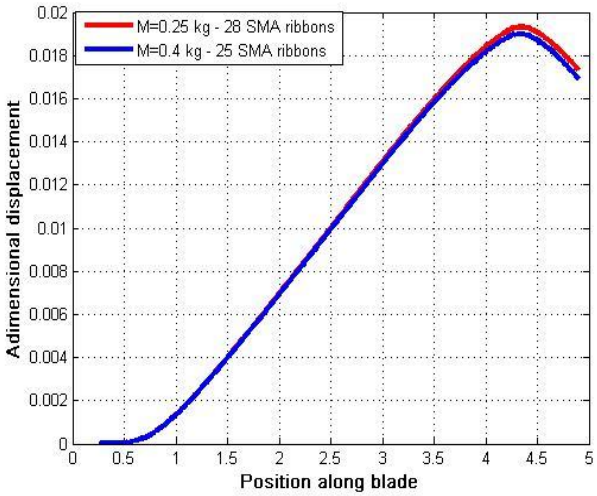

Figure 6: blade flap deformation with two SMA actuators.

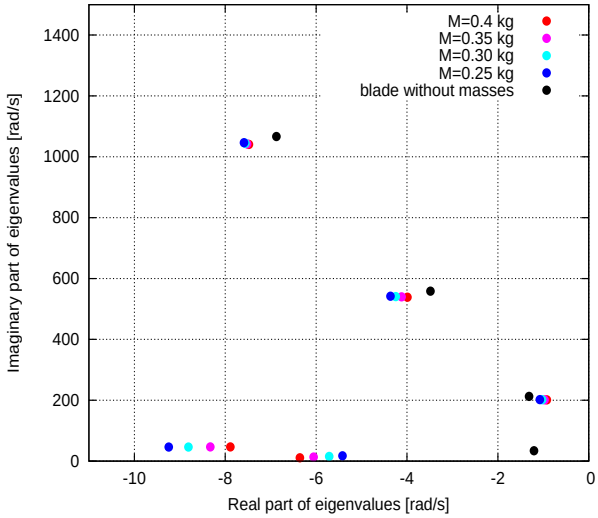

Figure 7: locus of roots for different values of M, for $T = 25000N$.

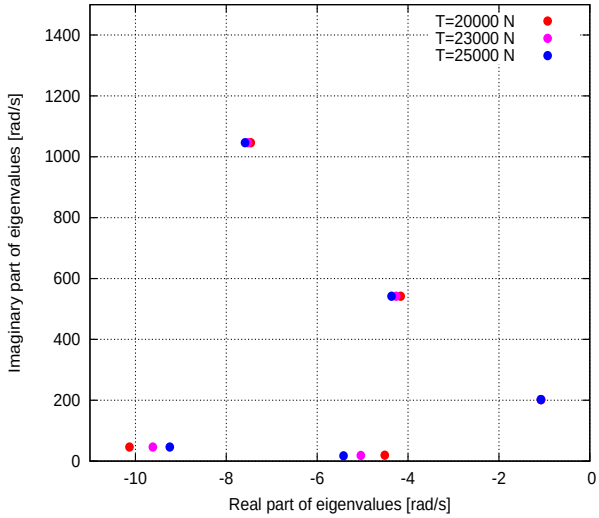

Figure 8: locus of roots for different values of T, for $M = 0.25Kg$.

The aeroelastic analysis has shown that, for a rotor thrust $T = 25000N$, the re-designed actuated smarted rotor is stable for the tip mass range examined, $0.25Kg < M < 0.4Kg$. In figure 7 the locus of the roots closer to the imaginary axis are depicted, along with the roots concerning the basic blade. Basic and actuated smarted blades have a similar critical damping, however it is interesting to observe that the actuation of the smart system yields a very damped lead-lag mode. For the actuated smarted blade the critical

damping slightly increases with the reduction of the tip mass. Fixing the tip mass value $M = 0.25Kg$, figure 8 shows that the effect of the rotor thrust, T, on the aeroelastic stability behavior is very small, with the critical damping unchanged. The beak profile obtained when M is between $0.25Kg$ and $0.4Kg$ could be not sufficient to reduce the BVI noise: the aeroelastic results show that, in this case, there is still space for the re-design of the blade aimed to an increase of the centrifugal actions. However, the inclusion of the

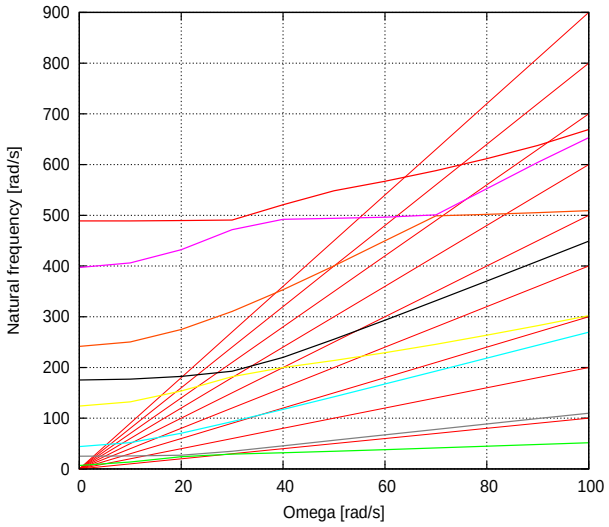

Figure 9: fan diagram for basic blade.

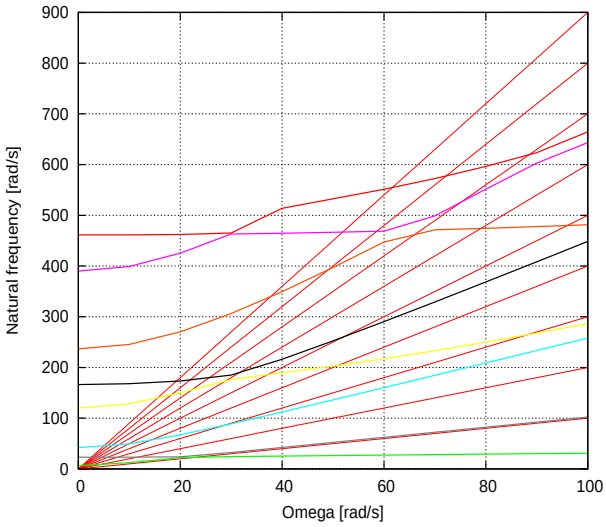

Figure 10: fan diagram for smarted blade.

smart device has an aeroelastic drawback: the lead-lag root becomes unstable when it is not actuated (and, thus, the concentrated masses are located at the lower side of the blade box). This instability occurs for any value of M in the examined range and, of course, is a critical issue in use of the smart system presented. The use of lag dampers could be a solution to this problem that, anyway, is a proof that the system needs additional reasearch activity.

Finally, results concerning the smarted rotor dynamic response is investigated. In particular, the attention is focused on the effects on the fan diagram of the system configuration with $M = 0.25Kg$. Figure 7 depict the fan diagram concerning the basic blade, whereas figure 8 shows the effects of the smart system on it. Some changes of the eigenvalues can be observed, but the overall dynamic behavior of the smarted blade is very similar to that of the basic blade and, in this context, the effect of the added masses is small.

5 CONCLUSIONS

In this paper the aeroelastic behavior of an innovative smart blade aimed to change the shape of the blade tip region has been investigated. The reduction of BVI noise is the goal of the morphing action. The motivation of the analysis comes from the fact that the effectiveness of the proposed system depends on the bending actions due to a set of concentrated masses located inside the blade box at the tip region, and thus their influence on the blade aeroelasticity and dynamic response may represent a limitation to the application of it. Some configurations of the smart system have been discussed and the efficiency of their morphing action demonstrated. For the activated system, configurations that assure aeroelastic stability have been identified, but they have shown to be unstable when the system in not activated and the added masses are locate below

the elastic axis. This is a drawback of the proposed morphing actuator that might be overcome by inserting suitable dampers, but this issue requires further investigations. The fan diagrams have shown that the inclusion of the smart system does not alter significantly the dynamic behavior of the blade, thus not introducing resonances. The effectiveness of the smart system in terms of noise abatement has not been studied and this aspect need to be analysed in future investigations, in order to define a smart configuration that is the best compromise between noise reduction and aeroelastic performance.

6 REFERENCES

[1] Prouty, R.W., "*Even More helicopter aerodynamics*", Phillips Pub. Co., 1993.

[2] Tung, C., and Lee, S., "*Evaluation of hover prediction codes*", Proceedings of the 50th Annual Forum of the Am. Hel. Soc., Washington, DC, May 11-13, 1994.

[3] Testa, C., Leone, S., Ameduri, S., Concilio, A., "Helicopter Blade Morphing: an Integrated Approach to Estimate the Capabilities of Complex Smart Materials-Based Architectures, submitted to the Journal of Intelligent Material Systems and Structures.

[4] Testa, C., Leone, S., Ameduri, S., Concilio, A., "*Feasibility Study on Rotorcraft Blade Morphing in Hovering*," Proceedings of International Symposium on Smart Structures and Materials, San Diego, California (USA), March, 2005.

[5] Bir, G., Chopra, I., et al., "*University of Maryland Advanced Rotor Code (UMARC) Theory manual*", Technical Report UM-AERO 94-18, Centre for Rotorcraft Education and Research, University of Maryland.

[6] Hodges, D.H. and Dowell, E.H., "*Nonlinear Equation for the Elastic Bending and Torsion of Twisted nonuniform Rotor Blades*," NASA TN D 7818.

[7] Hodges, D.H. and Ormiston, R., "*Stability of Elastic Bending and Torsion of Uniform Cantilever Rotor Blades in Hover with Variable Structural Coupling*," NASA TN 8192.

[8] Kwon, O.J., "*A technique for the prediction of aerodynamics and aeroelasticity of rotor blades*," PhD Thesis, Georgia Institute of Technology, 1988.

[9] Splettstoesser, W.R., Niesl, G., Cenedese, F. and Papanikas, D.G., "*Experimental Results of the European HELINOISE Aeroacoustic Rotor Test in the DNW*," Proceedings of the 19th European Rotorcraft Forum, Cernobbio, Italy, September, 1993.